Histol Histopathol (2024) 39: 921-934

Histology and Histopathology
From Cell Biology to Tissue Engineering

ORIGINAL ARTICLE Open Access

Inflammatory suppression and immunity regulation benefits of honokiol in a rat model of acute peritonitis via the regulation of NLRP3 inflammasome and Sirt1/autophagy axis

Ximing Pan[1], Zhou Hua[2], Guocai Fan[3] and Qinglong Feng[4]

[1]Department of Emergency, [2]Department of Nephrology, [3]Department of Breast Surgery, Suichang People's Hospital, Lishui and [4]Intensive Care Unit, Quzhou Kecheng People's Hospital, Quzhou, PR China

Summary. Background. NLRP3 inflammasome and Sirt1/autophagy axis are potential targets for advancing acute peritonitis (AP). Honokiol (HNK), a bioactive substance, has the potential to improve AP.

Materials and methods. The AP model rats were established by cecal ligation and puncture (CLP). Rats were randomized into the Sham, Sham+HNK, CLP, and CLP+HNK groups. The therapeutic effects of HNK on organ infection, inflammation and immunity were observed in AP rats. The inflammation of RAW 264.7 cells was induced by lipopolysaccharide (LPS) and divided into the Control, HNK, LPS, and LPS+HNK groups. The effects of HNK on immunity and inflammation were observed. Moreover, the inflammatory cell model was further transfected with NLRP3 overexpressing plasmid, and the regulatory effect of HNK on NLRP3 in AP cells was detected.

Results. HNK treatment improved survival, biochemical indexes, and lung and kidney injury and inhibited inflammatory cytokine release and bacterial infection in CLP rats. In CLP rats and RAW 264.7 cells, HNK treatment improved the release of the CD4+ and CD8+ T cells, decreased the associated proteins' levels of the NLRP3 inflammasome, and activated the expression of proteins in the Sirt1/autophagy axis. It improved viability and reduced apoptosis and the degrees of TNF-α, IL-1β, and IL-6 mRNA in RAW 264.7 cells. In addition, HNK treatment antagonized the effect of NLRP3-overexpressed on inflammation and immunity.

Conclusions. HNK improved AP by inhibiting NLRP3 inflammasome and activating the Sirt1 autophagy axis *in vivo* and *in vitro*.

Corresponding Author: Qinglong Feng, Intensive Care Unit, Quzhou Kecheng People's Hospital, Quzhou 324000, PR China. e-mail: qinglongfengicu@sina.com

www.hh.um.es. DOI: 10.14670/HH-18-688

Key words: Acute peritonitis, Honokiol, NLRP3, Sirt1, Cecal ligation and puncture (CLP), Lipopolysaccharide (LPS)

Introduction

Acute peritonitis (AP), with high morbidity and mortality, is a disease with a serious inflammatory response caused by bacterial infection, chemical stimulation, or tissue damage, and is also the main reason leading to sepsis (Boland et al., 2011). It is accompanied by a variety of acute tissue injuries, such as acute kidney injury and acute lung injury (Rodrigues et al., 2018). During the onset of peritonitis, there is a large amount of apoptosis of macrophages, and a sharp increase in proinflammatory cytokines, such as interleukin-6 (IL-6) and tumor necrosis factor α (TNF-α) in serum (Kolaczkowska et al., 2010; Mikhalchik et al., 2020). The overall increase in proinflammatory factors can lead to uncontrolled inflammation, resulting in significant end-organ damage and death (Chakraborty and Burns, 2022). Studies have proposed that NOD-like receptor thermal protein domain-associated protein 3 (NLRP3) inflammasomes have been activated in the peritonitis model and have participated in the inflammatory response, resulting in damage to peritoneal structure and function (Hautem et al., 2017). Enhanced autophagy can block inflammasome-mediated

Abbreviations. AP, Acute peritonitis; HNK, Honokiol; CLP, Cecal ligation and puncture; LPS, Lipopolysaccharide; NLRP3, NOD-like receptor thermal protein domain associated protein 3; SD, Sprague-Dawley; qRT-PCR, Quantitative real-time PCR; ALT, Alanine aminotransferase; AST, Aspartate aminotransferase; Scr, Serum creatinine; BUN, Blood urea nitrogen; LDH, Lactate dehydrogenase; CK-MB, Creatine kinase-MB; TNF-α, Tumor necrosis factor α; IL-1β, Interleukin-1β; IL-6, Interleukin-6; MCP-1, Monocyte chemoattractant protein-1

inflammatory diseases (Youm et al., 2015), and also degrade intracellular pathogens and endogenous substrates to regulate immunity (Metur and Klionsky, 2021). Sirtuin1 (Sirt1) is a target that regulates autophagy and apoptosis (Nurmi et al., 2017). A study reported that Sitr1 deacetylates Beclin1 to attenuate acute kidney injury in cecal ligation and puncture (CLP) mice. Beclin1 is a mammalian autophagy protein (Deng et al., 2021). Additionally, Wu and co-workers reported that Sirt1-mediated autophagy attenuated the activation of NLRP3 inflammasome to improve IgA nephropathy (Wu et al., 2020). Scientists also reported that upregulation of Sirt1-related signaling pathways inhibited inflammatory factors in CLP mice and lipopolysaccharide (LPS)-treated RAW 264.7 cells (Wang et al., 2022). In a word, NLRP3 and Sirt1 may be the key to the effective prevention and treatment of AP (Doklestić et al., 2014).

Honokiol ($C_{18}H_{18}O_2$) (HNK) is a bioactive substance with anti-inflammatory, antioxidative stress, and antithrombotic properties extracted from *Magnoliae Officinalis Cortex* (Zhang and Shen, 2021). It's a member of the biphenyls compound with a para-allyl phenol and an ortho-allyl phenol joined together with the ortho-, para-C-C-coupling (Li et al., 2022). In recent years, researchers have found that HNK has good antibacterial and anti-inflammatory potential *in vitro*, and it could reduce CLP-induced inflammatory cytokine production (Xia et al., 2019; Chiu et al., 2021). Yang's team proposed that HNK has enhanced the Sirt1/autophagy axis and inhibited the NLRP3 inflammasome, which played an inhibitory role in the inflammatory response (Yang et al., 2020). However, the biological mechanism of NHK in AP is still lacking. Based on this, by constructing the CLP rat model and LPS-treated inflammatory cell model, this study aims to explore the biological effects of HNK on CLP by regulating autophagy and inhibiting inflammation *in vivo* and *in vitro*.

Materials and methods

Animals and CLP modeling

The animals were Sprague-Dawley (SD) rats (200-230 g) purchased from Shanghai Jihui Laboratory Animal Care Co., Ltd. The Animal Experimentation Ethics Committee of Zhejiang Eyong Pharmaceutical Research and Development Center (SYX (Zhe) 2021-0033) reviewed and approved all animal-related work for this study. The rats were raised with sufficient standard feed and water, at 60±10% humidity and 20±2°C temperature, and the environment was circulated day and night for 12h. The rats were randomized into 4 groups, which were named the Sham, the Sham+HNK, the CLP, and the CLP+HNK group with 16 animals in each group. SD rats in the CLP and CLP+HNK groups were anesthetized with isoflurane and then cut from the middle of the abdominal wall, gently pulling out the cecum to avoid damaging the mesenteric vessels and separating mesenteric surface vessels. The cecal valve was ligated at the midpoint of the cecum with sterile No. 4 thread, and the perforation at the midpoint between the ligation site and the top of the cecum was punctured with a 21 G sterile needle. Then the cecum was put back into the abdominal cavity and sutured (Liu et al., 2022b). Subsequently, resuscitation and relieving of pain were carried out with 5 mL/100 g of normal saline and buprenorphine (0.05 mg/kg). The animal-related molding work in the Sham and Sham+HNK groups was like those in the CLP and CLP+HNK group except that they did not ligate and puncture the cecum. Within 24h after the operation, all rats were injected intraperitoneally with HNK (5 mg/kg twice) (≥98%, B20511, Yuanye, Shanghai, CHN) or PBS in the same volume. Survival rates of ten rats at 0, 24, 48, 72, 96, and 120h after operation were observed and counted.

Cells and treatment

Macrophage strain (RAW 264.7) was bought from iCell Bioscience Inc, Shanghai, China, and grown in Dulbecco's modified Eagle's medium (SH30243.01, HyClone, Utah, US), with 10% fetal bovine serum (11011-8615, Every Green, Zhejiang, CHN), 37°C, and 5% CO_2. The cells were grouped as follows, the Control (CN) group without any treatment; the HNK group was cultured with HNK for 24h; cells in the LPS group were cultured with the lipopolysaccharide (LPS) for 24h (S11060, Yuanye, Shanghai, CHN); the LPS+HNK group was treated with HNK and LPS for 24h. The dosage of HNK was 50 μM and LPS was 10 μg/mL.

In the LPS+EV group, the empty vector-transfected cells were treated with LPS for 24h; in the LPS+HNK+EV group, the empty vector-transfected cells were treated with HNK and LPS for 24h; in the LPS+NLRP3 group, the RAW 264.7 cell line with the NLRP3 overexpression was treated with LPS for 24h; the LPS+HNK+NLRP3 group performed the same operations as the LPS+NLRP3 group besides additional HNK pretreatment.

NLRP3 overexpression cell lines were established using the Lipofectamine 3000 kit (L3000-015, Invitrogen, CA, US) according to the instructions. The plasmid vector containing the NLRP3 DNA or empty vector plasmid (pcDNA3.1/CT-GFP-TOPO, Invitrogen, CA, US) was mixed with the cells and cultured for 48h.

Plasmid construction

The cDNA of NLRP3 was extracted from RAW 264.7 cells and subjected to quantitative real-time PCR (qRT-PCR). The sequenced primer sequences are GFP forward 5'-CGACAAATCTGCCCTTTCG-3' and bGH reverse 5'-TAGAAGCACAGTCGAGG-3'. The cDNA or empty vector plasmid was digested by restriction

enzyme (KpnI/NotI, NEB, MA, US), the gene was purified by a DNA purification kit (BBI, Shanghai, CHN) and was transformed into competent cells. After the competent cells were expanded culture, a single clone colony was taken from them for PCR at 95°C for 5 min, 95°C for 30 s, 58°C for 30 s and 72°C. Finally, the positive cloning results were sent for sequencing analysis. The sequence number of mouse NLRP3 gene obtained from the NCBI database is 216799.

Serum and tissue collection

After anesthesia with 2% pentobarbital sodium, blood was collected from the left ventricle. After blood collection, the rats were euthanized with CO_2. Perfusion was performed immediately after confirmation of complete death. Rats were perfused with pre-cooled PBS to remove the kidney and lung. Tissues were embedded in paraffin or stored at -80°C. The above operations were performed by professional technicians. Blood was used to prepare serum and determine biochemical indexes: alanine aminotransferase (ALT), aspartate aminotransferase (AST), serum creatinine (Scr), blood urea nitrogen (BUN), lactate dehydrogenase (LDH), and creatine kinase-MB (CK-MB).

Histological Assessment by hematoxylin-eosin staining (HE)

After dewaxing, the sections made of tissue paraffin blocks were stained with HE kits (G1003, SERVICEBIO, Wuhan, CHN) according to the product guidelines, and then observed with a microscope (Nikon Eclipse, JPN) after sealing. The samples were scored according to the degree of inflammatory cell infiltration and the level of swelling and desquamation of epithelial cells. Normal was 0 points and 1 point was given for infiltration of a few inflammatory cells, with no swelling and desquamation of epithelial cells. A score of 2 indicates that inflammatory cell infiltration is clearly observed with a few epithelial cells swelling and desquamation; a score of 3 indicates more epithelial cells swelling and desquamation; a score of 4 indicates massive inflammatory cell infiltration and numerous epithelial cells swelling and desquamation.

Detection of the biochemical index and proinflammatory factors in serum

The levels of LDH, CK-MB, ALT, AST, SCR, and BUN were measured by the automated biochemical detector (C16000, Abbott, ME, US). The degrees of proinflammatory cytokine secretion were detected by ELISA. The ELISA kits for TNF-α (MM-0132M1), interleukin-1β (IL-1β) (MM-0040M1), interleukin-6 (IL-6) (MM-0190R1), and monocyte chemoattractant protein-1 (MCP-1) (MM-0099R1) were purchased from MEIMIAN Industrial Co., Ltd., Jiangsu, China.

Bacterial culture of blood and peritoneal fluid

Rat blood and peritoneal fluid were collected under sterile conditions. After 10 times gradient dilutions, they were plated on the blood agar plate for bacterial culture and colony count.

Flow cytometry assay

The spleen was cleaned with PBS (2% penicillin-streptomycin) to remove connective tissue, and the cells were screened by squeezing through a sieve (200 μm). The cells were placed in a 15 mL centrifuge tube for centrifugation, then the sediment was removed and made into a 2×10^7/mL suspension. The 100 μL suspension was incubated with 2.5 μL of anti-rat CD3 (554833), anti-rat CD4 (550057), and anti-rat CD8a (561965) antibodies that were bought from Becton, Dickinson and Company, CA, USA, or anti-mouse CD86 (B7-2) (F2108601) that was bought from MultiSciences Biotech Co., Ltd, Hangzhou, China at 4°C away from light for 30 min. After cleaning, suspending, and re-sieving, the assay was performed on a BD Accuri™ C6 flow cytometer (BD, NJ, US).

Western blot

The proteins of tissues and cells were extracted with RIPA lysis buffer (P0013D, Beyotime, Shanghai, CHN) and the concentration of proteins was assessed by a BCA kit (pc0020, Solarbio, Beijing, CHN). The protein with loading buffer (the volume ratio was 1:4) was incubated in 100°C boiling water for 5 min. The samples were differentiated in SDS-PAGE concentrated rubber by electrophoresis. Later, they were transferred to the polyvinylidene fluoride membrane by electroblotting. Subsequently, 5% non-fat milk was used to block the samples. After washing, they were incubated with the antibody lists at the end of the paragraph at 4°C overnight. They were then washed by TBST. Subsequently, the samples reacted with anti-rabbit IgG (7074, CST, MA, US) for 2h at 25°C. Then the film was washed again. After the film was treated with ECL chemiluminescence kits (PE0010, Solarbio, Beijing, CHN), it was imaged using a chemiluminescence instrument (610020-9Q, Qinxiang, Shanghai, CHN). Primary antibodies included NLRP3 (AF4620), Sirt1 (AF6474), Beclin1 (AF5128), LC3 A/B (AF5402), GAPDH (AF7021) provided by Affinity Biosciences Ltd., Co, Jiangsu, China.

MTT colorimetric assay

Log-phase RAW 264.7 cells (2×10^4/mL) were cultured into 96-well plates and processed based on grouping. After that, 20 μL/well 3- (4,5-dimethylthiazol-2-yl)-2,5-diphenyltetrazolium bromide (MTT) (5 mg/mL) (Sigma-Aldrich, Merck KGaA) was added to

react at 37°C, lasting for 4h. DMSO was added at 200 μL/well into the formed products and the optical density (OD) was measured at 490 nm using a CMaxPius microplate reader (SpectiaMax, US).

TUNEL staining

The cells were grown on the covered glass until a cell confluence of 60-70%, and the cells were treated according to grouping. The culture medium was then discarded, and the cells were washed. The cells were fixed with 4% paraformaldehyde for 30 minutes and immersed in PBS for 5 minutes. After the cell membrane was permeated with 0.3% Triton X-100, the cells were processed with the TUNEL kit (C1090, Beyotime, Shanghai, CHN). Between each step, the cells were washed in PBS 3 times for 5 min each time. Finally, the cells were sealed and analyzed under inverted fluorescence microscopy (Ts2-FC, Nicon, JPN). The red fluorescent dots in the image represent positive cells, and the results were analyzed by the ratio of positive cells to total cells.

Cellular immunofluorescence (IF) assay

The cells were inoculated and fixed. 3% BSA was blocked in cells for 30 min. The cells were added with the NLRP3 antibody (DF7438, Affinity, Jiangsu, CHN) and kept away from light at 4°C for one night. After washing with PBS for 5 min/time, the cells were reacted with the goat anti-rabbit IgG H&L (Alexa fluor® 488) (ab150077, Abcam, Cambs, UK) in dark for 30 min at 25°C. The cells were then washed again and DAPI was added. The samples, after being cleaned with BSA and mounted with mounting media were observed under an inverted fluorescence microscope.

qRT-PCR

Cells were lysed with Trizol (B511311, Sangon Biotech, Shanghai, CHN) and centrifuged to retain the supernatant. The supernatant was successively treated with chloroform and isopropanol successively to obtain precipitation, centrifuged after each treatment, and finally the precipitation was rinsed with 75% absolute ethanol. The RNA was dissolved in 40 μL of DEPC water and stored in a -80°C refrigerator for standby. Reverse transcription process was performed using the HiFiScript cDNA Synthesis Kit (CW2569, cwbio, Beijing, CHN). Reaction conditions: 42°C for 15 min; 85°C for 5 min. Finally, the qRT-PCR was performed with the SYBR Premix Ex TaqII (RR820A, Takara, JPN) according to the following procedure: at 95°C for 10 min and 95°C for 15 s, then at 60°C for 60 s, performed 40 cycles. Data were processed by the relative quantitative method ($2^{-\Delta\Delta Ct}$). Primer sequences are shown in Table 1.

Statistical analyses

One-way analysis of variance (ANOVA) with the *post hoc* Tukey test was used between multiple groups of measurement data. In addition, the student's t-test was used to compare data between two groups with normal distribution and equal variance. All analyses were performed with SPSS 16.0 (IBM, USA). Data are presented as mean (SD), $p<0.05$ the difference was statistically significant.

Results

HNK improved the survival rate and biochemical indexes in CLP rats

The survival rate of rats was significantly lower in the CLP group (10%) compared to the Sham group (100%) at 120h ($p<0.01$). However, the CLP+HNK group showed a higher survival rate (40%) compared to the CLP group (10%) at 120h ($p<0.01$). Compared to the Sham group, the survival rate of rats in the Sham+HNK (100%) group did not show a pronounced difference. (Fig. 1A)

In addition, serum biochemical indexes in rats reflecting the severity of organ damage were detected. The findings exhibited that the degrees of ALT, AST, SCr, and BUN in the Sham+HNK group were not significantly different from those in the Sham group ($p>0.05$). ALT, AST, SCr, and BUN levels in the CLP group were elevated in comparison with the Sham group ($p<0.01$). Additionally, the CLP+HNK group showed suppressed ALT, AST, SCr, and BUN levels in comparison with the CLP group ($p<0.01$) (Fig. 1B-G).

HNK alleviated the tissue damage to the lung and kidney in CLP rats

Histopathologic alterations in the lungs and kidneys of CLP rats were observed using HE. The structure of the lungs in the Sham group appeared physiologically normal and clear. Compared to the Sham group, there was no pronounced change in the lung tissue in the

Table 1. Primer sequence.

Gene	Forward Primer (5'-3')	Reverse Primer (5'-3')
Mouse TNF-α	CAGGCGGTGCCTATGTCTC	CGATCACCCCGAAGTTCAGTAG
Mouse IL-6	TCCGGAGAGGAGACTTCACA	CATAACGCACTAGGTTTGCCG
Mouse IL-1β	AAGGGGACATTAGGCAGCAC	ATGAAAGACCTCAGTGCGGG
Mouse GAPDH	AGGTCGGTGTGAACGGATTTG	GGGGTCGTTGATGGCAACA

Sham+HNK group (Fig. 2A). Conversely, the CLP group exhibited evident inflammatory cell infiltration, marked tracheal wall thickening, and irregularities in comparison to the Sham group. However, the number of inflammatory cells in the CLP+HNK group decreased, and there was some obvious lumen structure compared with the CLP group. According to the infiltration area of inflammatory cells and swelling and desquamation of epithelial cells, the severity of histopathological injury was scored semi-quantitatively. Results are displayed in Figure 2B. The scores of the Sham+HNK group had no meaningful difference ($p>0.05$), while the scores of the CLP group were significantly higher than those of the Sham group ($p<0.01$). In the CLP+HNK group, the lung histopathology score was reduced by 35% compared to the CLP group ($p<0.01$).

Regarding the kidney, no significant pathological changes were observed in the Sham group (Fig. 2A,C). There were no remarkable differences in renal histopathology of the kidney between the Sham+HNK group and the Sham group. While numerous brown crystals in the CLP group were deposited in the renal tubules, the structure of renal tubules was destroyed, and many inflammatory cells were found to have infiltrated, the score of which was notably higher than that of the Sham group ($p<0.01$). On the other hand, compared with the CLP group, the cell morphology of the CLP+HNK group was improved and the histopathologic score of the kidney was reduced by 33% ($p<0.01$).

HNK inhibited the bacterial growth and inflammation in CLP rats

The bacterial culture levels in rat blood and peritoneal fluid showed a significant increase in the CLP group compared to the Sham group ($p<0.01$). However, CLP rats that were treated with HNK showed significantly lower bacterial cultures ($p<0.01$) (Fig. 2D,E).

The expression levels of proinflammatory cytokines such as TNF-α, IL-1β, IL-6, and MCP-1 were detected by ELISA. The results in the CLP group were all higher

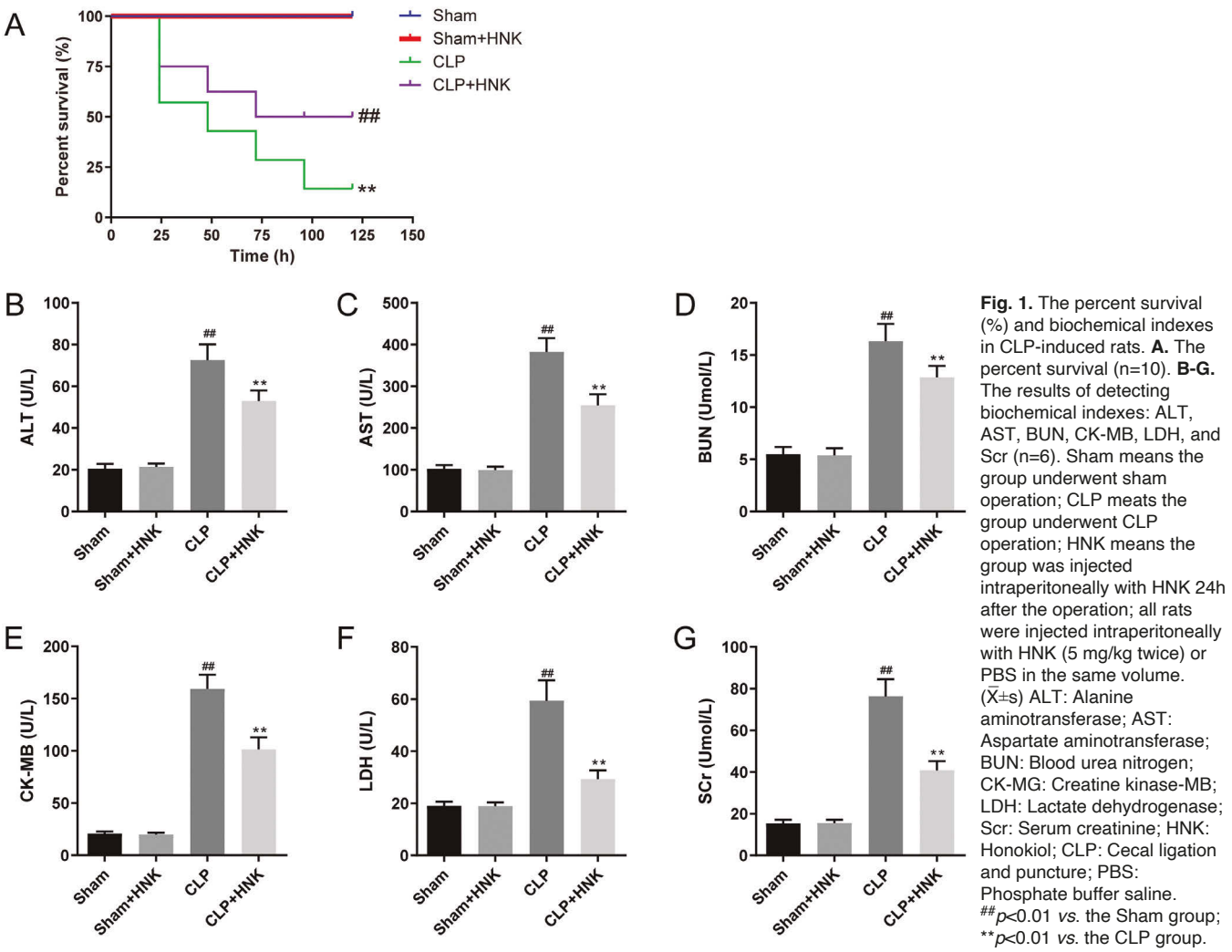

Fig. 1. The percent survival (%) and biochemical indexes in CLP-induced rats. **A.** The percent survival (n=10). **B-G.** The results of detecting biochemical indexes: ALT, AST, BUN, CK-MB, LDH, and Scr (n=6). Sham means the group underwent sham operation; CLP meats the group underwent CLP operation; HNK means the group was injected intraperitoneally with HNK 24h after the operation; all rats were injected intraperitoneally with HNK (5 mg/kg twice) or PBS in the same volume. ($\bar{X}\pm s$) ALT: Alanine aminotransferase; AST: Aspartate aminotransferase; BUN: Blood urea nitrogen; CK-MG: Creatine kinase-MB; LDH: Lactate dehydrogenase; Scr: Serum creatinine; HNK: Honokiol; CLP: Cecal ligation and puncture; PBS: Phosphate buffer saline. ##$p<0.01$ *vs.* the Sham group; **$p<0.01$ *vs.* the CLP group.

than those in the Sham group ($p<0.01$), and those in the CLP+HNK group were all lower than those in the CLP group ($p<0.01$) (Fig. 2F-I).

HNK improved the level of splenic CD3+ CD4+ and CD3+ CD8+ T lymphocytes in CLP rats

To evaluate the impact of HNK on the immune function of CLP rats, the T lymphocytes percentages in rat splenocytes were detected by flow cytometry. The expression degrees of $CD3^+$ $CD4^+$ and $CD3^+$ $CD8^+$ T lymphocytes were significantly lower in the CLP group than those in the Sham group ($p<0.01$), whereas in the CLP+HNK group, the percentages were significantly higher compared to those in the CLP group ($p<0.05$ and $p<0.01$) (Fig. 3A,B).

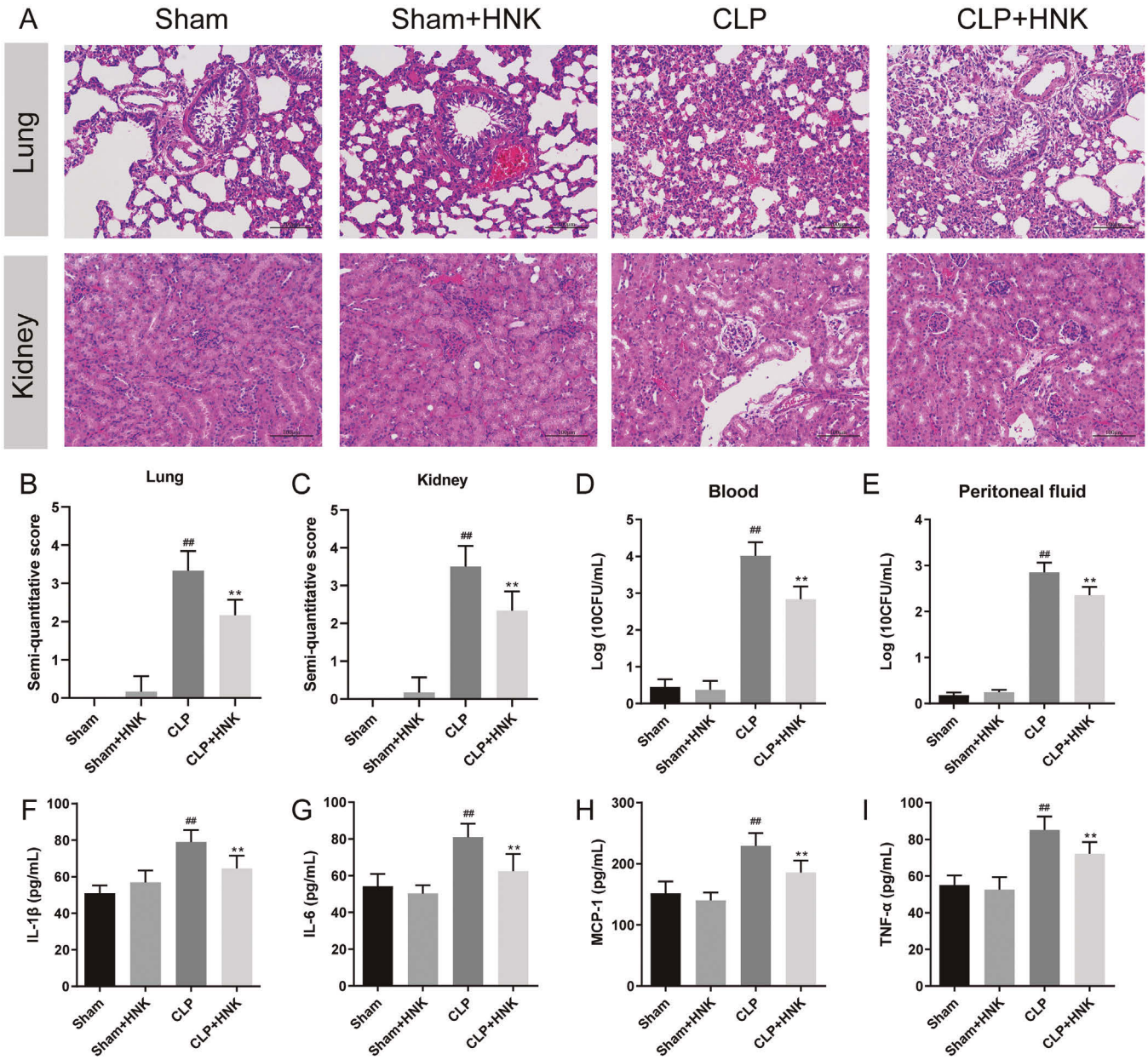

Fig. 2. Hematoxylin-eosin staining of lung and kidney, number of bacteria and levels of inflammatory factors in CLP-induced rats. ($\bar{X}$±s, n=6). **A-C.** Hematoxylin-eosin staining of lung and kidney. Scale bar: 100 μm). **D.** Number of bacteria in blood. **E.** Number of bacteria in peritoneal fluid. **F-I.** The levels of IL-1β, IL-6, MCP-1 and TNF-α by ELISA. Sham means the group underwent sham operation. Sham means the group underwent sham operation; CLP meats the group underwent CLP operation; HNK means the group was injected intraperitoneally with HNK 24h after the operation; all rats were injected intraperitoneally with HNK (5 mg/kg twice) or PBS in the same volume. HNK: Honokiol; CLP: Cecal ligation and puncture; PBS: Phosphate buffer saline. $^{\#\#}p<0.01$ *vs.* the Sham group; $^{**}p<0.01$ *vs.* the CLP group.

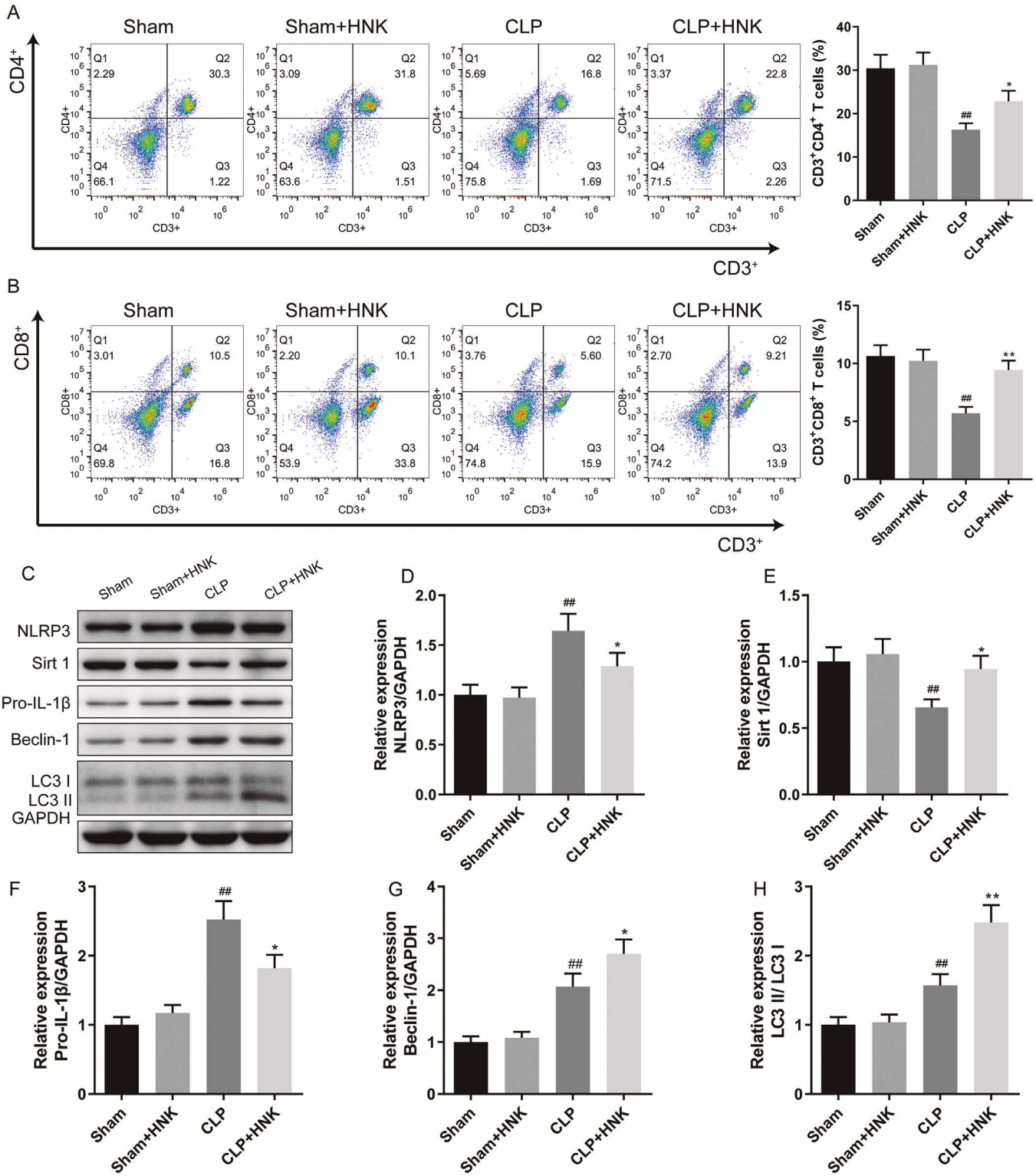

Fig. 3. The level of splenic CD4$^+$ and CD8$^+$ T lymphocytes and the expression of related proteins of NLRP3 inflammasome and Sirt1/autophagy axis in CLP rat. ($\bar{X}\pm s$, n=3). **A.** The CD4$^+$ T cells in spleens of CLP rats by flow cytometry. **B.** The CD8$^+$ T cells in spleens of CLP rats by flow cytometry. **C.** Bands of proteins; **D-H.** The statistical analysis results of NLRP3, Sirt1, Pro-IL-1β, Beclin-1, and LC3 II/LC3 I proteins bands by Western blot. Sham means the group underwent sham operation; CLP meats the group underwent CLP operation; HNK means the group was injected intraperitoneally with HNK 24h after the operation; And all rats were injected intraperitoneally with HNK (5 mg/kg twice) or PBS in the same volume. HNK: honokiol; CLP: cecal ligation and puncture; PBS: Phosphate buffer saline; NLRP3: NOD-like receptor thermal protein domain associated protein 3; Sirt1: Sirtuin1; Pro-IL-1β: Pro-Interleukin-1β; LC3: MAP1LC3. $^{\#\#}p<0.01$ *vs.* the Sham group; $^*p<0.05$, $^{**}p<0.01$ *vs.* the CLP group.

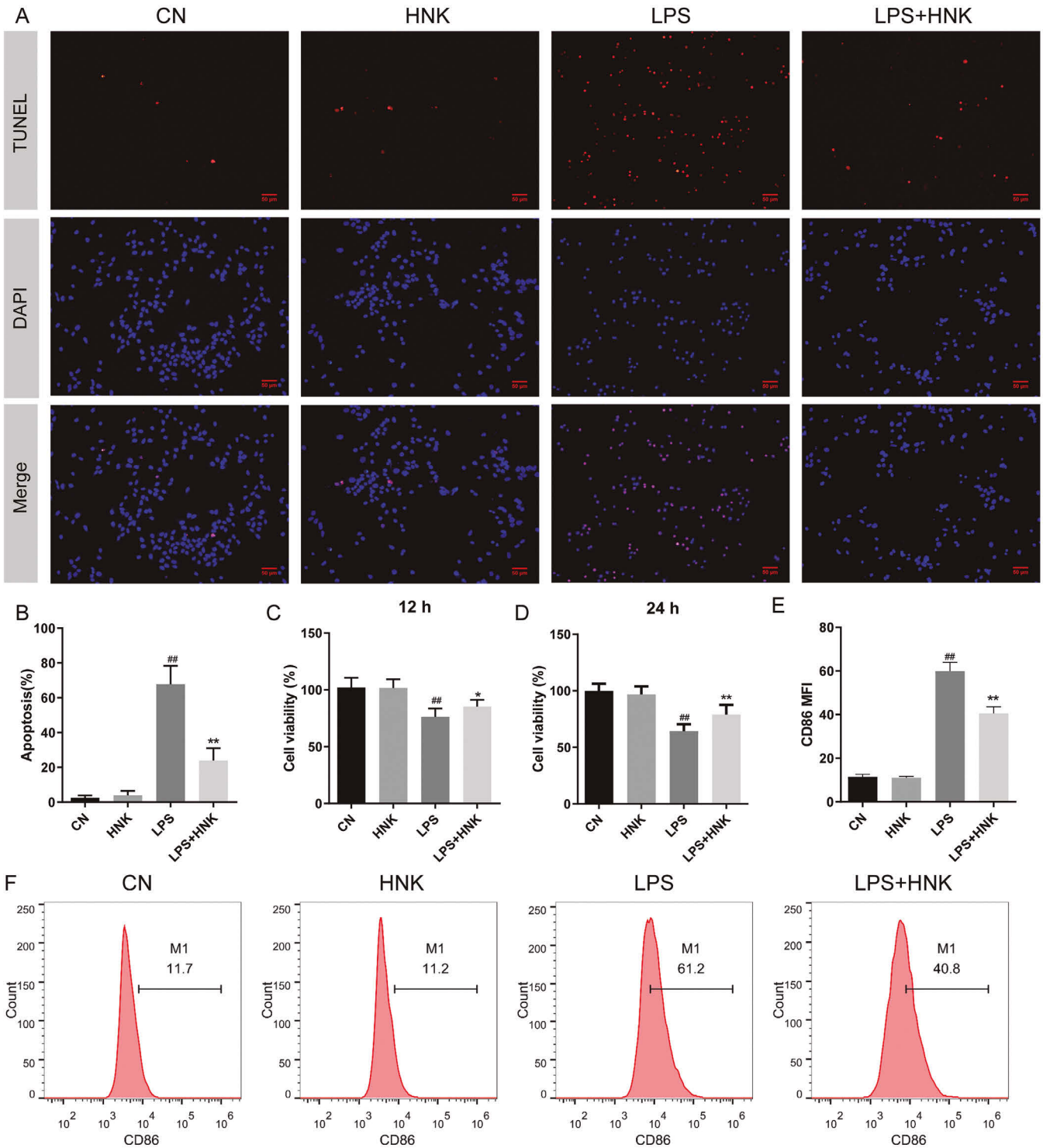

Fig. 4. The apoptosis, viability and the proportion of CD38^{+} cells in RAW 264.7 cells. (x400, $\bar{X}\pm s$). **A, B.** Representative photos of TUNEL and the apoptosis rate (%) was analyzed from the results of TUNEL. The red fluorescent dots in the image represent positive cells, and the results were analyzed by the ratio of positive cells to total cells (n=3). **C, D.** The cell viability in RAW 264.7 cells for 12h and 24h by MTT colorimetric assay (n=6). **E, F.** The CD38 MFI in RAW 264.7 cells were detected by flow cytometry (n=3). The CN group without any treatment; the HNK group was cultured for 24h with HNK (50 μM); the LPS group was cultured for 24h with the lipopolysaccharide (LPS) (10 μg/mL); the LPS+HNK group was treated with HNK and LPS for 24h. CN: Control; MTT: [3-(4,5-dimethylthiazol-2-yl)-2,5-diphenyltetrazolium bromide; HNK: honokiol; LPS: lipopolysaccharide; MFI: mean fluorescence intensity. $^{\#\#}p<0.01$ *vs.* the CN group; $^{*}p<0.05$, $^{**}p<0.01$ *vs.* the LPS group.

HNK affected the expression of related proteins of NLRP3 inflammasome and Sirt1/autophagy axis in CLP rats

The levels of NLRP3 inflammasome and Sirt1/autophagy axis proteins in the lung were analyzed by WB. Compared to the Sham group, the CLP group showed a 1.68-fold increase in the NLRP3 protein signal strength, a 2.15-fold increase in Pro-IL-1β protein expression, a 1.9-fold increase in Beclin-1 protein expression, and a nearly 51% increase in the LC3 II/LC3 I ratio (p<0.01) (Fig. 3D,F-H). In the CLP group, Sirt1 protein was reduced by 38% compared to the Sham group (p<0.01) (Fig. 3E). Conversely, in the CLP+HNK group, the levels of NLRP3 and Pro-IL-1β protein decreased by almost 21% and 28%, compared to the CLP group (p<0.01) (Fig. 3D,F). Moreover, in the CLP+HNK group, Sirt1, Beclin-1, and LC3 II/LC3 I proteins expressions showed a 1.44-fold, 1.3-fold, and 1.6-fold increase, respectively, compared to the CLP group (p<0.05 and p<0.01) (Fig. 3E,G-H).

HNK inhibited the apoptosis and improved the viability in LPS-stimulated RAW 264.7 cells

By TUNEL, this study observed the level of apoptosis. Compared to the CN group, there was no noteworthy difference in the HNK group (p>0.05). In the LPS group, the nuclei of cells were pyknotic (blue), some of those were fragmented, and the apoptosis rate was increased by a factor of 17.33-fold compared to the CN group (p<0.01). There was no significant change in shape and size of the nucleus of the LPS+HNK group compared with the LPS group, but the cell apoptosis rate was reduced by 65% (p<0.01) (Fig. 4A,B).

RAW 264.7 cell viability was measured using MTT assay. Results demonstrated that the viability of the HNK group at 12h and 24h did not show significant difference from the CN group (p>0.05). In contrast, the LPS group displayed a 25% and 34% reduction in cell

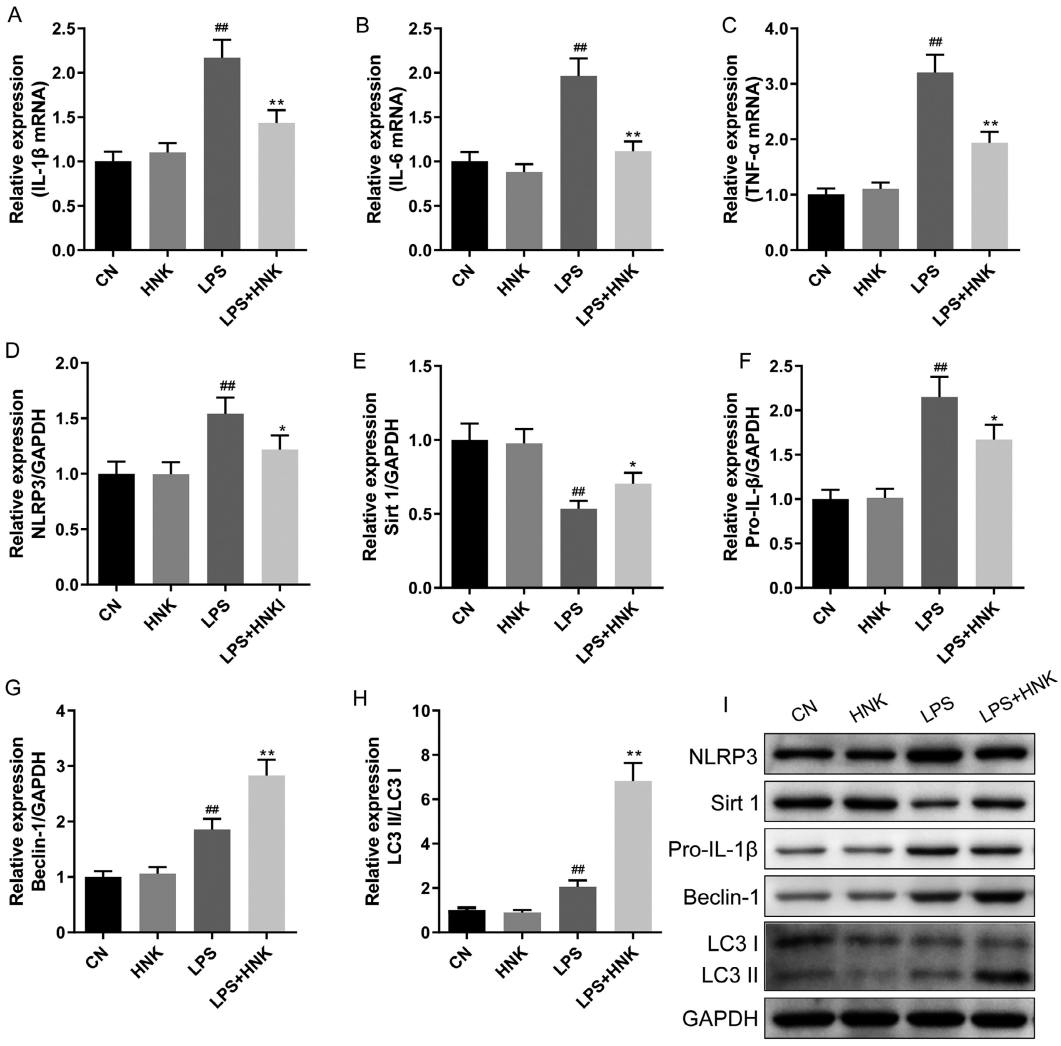

Fig. 5. The levels of TNF-α, IL-1β and IL-6 mRNA and related proteins of NLRP3 inflammasome and Sirt1/autophagy axis in RAW 264.7 cells ($\bar{X}$±s, n=3). **A-C.** The levels of TNF-α, IL-1β and IL-6 mRNA were measured by quantitative real-time PCR. **D-I.** The levels of NLRP3, Sirt1, Pro-IL-1β, Beclin-1, and LC3 II/LC3 I proteins were measured by Western blot. The Control (CN) group without any treatment; The HNK group was cultured for 24h with HNK (50 μM); the LPS group was cultured for 24h with the LPS (10 μg/mL); the LPS+HNK group was treated with HNK and LPS for 24h. TNF-α: Tumor necrosis factor-α; IL: Interleukin; NLRP3: NOD-like receptor thermal protein domain associated protein 3; Sirt1: Sirtuin1; LC3: MAP1LC3; HNK: honokiol; LPS: lipopolysaccharide. $^{\#\#}p$<0.01 *vs.* the CN group; $^{*}p$<0.05, $^{**}p$<0.01 *vs.* the LPS group.

viability at 12h and 24h, respectively, compared to the CN group (p<0.01). Furthermore, the LPS+HNK group exhibited a factor of 1.115-fold and 1.227-fold increase in cell viability at 12h and 24h, compared to the LPS group (p<0.05 and p<0.01) (Fig. 4C,D).

HNK inhibited inflammatory phenotypein in LPS-stimulated RAW 264.7 cells

CD86 is a marker for M1 macrophages, and M1 macrophages are involved in promoting inflammatory damage in sepsis (Jiao et al., 2021). CD86 levels in RAW 264.7 cells were determined by flow cytometry. The mean fluorescence intensity (MFI) was used for statistical analysis. The MFI indicates a significant increase in results for the LPS group compared to the CN group (p<0.01). Conversely, the results for the LPS+HNK group were notably lower than the LPS group (p<0.01) (Fig. 4E,F).

The inflammatory factor transcription levels in LPS-stimulated RAW 264.7 cells were measured by qRT-PCR. The qRT-PCR results, demonstrated in Figures 5A-C, exhibit an elevation in TNF-α, IL-1β, and IL-6 mRNA when compared to the CN group (p<0.01).

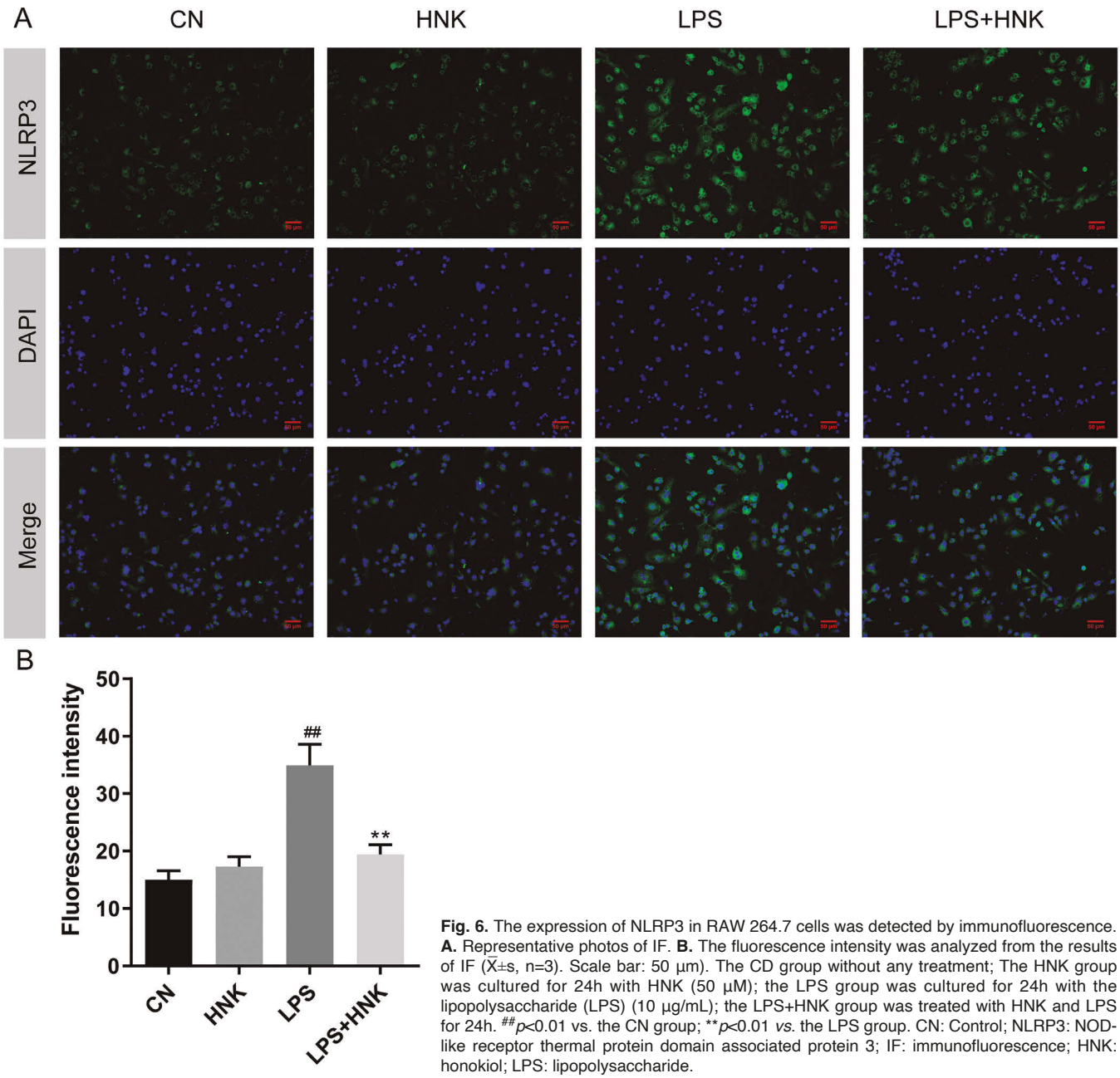

Fig. 6. The expression of NLRP3 in RAW 264.7 cells was detected by immunofluorescence. **A.** Representative photos of IF. **B.** The fluorescence intensity was analyzed from the results of IF ($\bar{X}\pm s$, n=3). Scale bar: 50 μm). The CD group without any treatment; The HNK group was cultured for 24h with HNK (50 μM); the LPS group was cultured for 24h with the lipopolysaccharide (LPS) (10 μg/mL); the LPS+HNK group was treated with HNK and LPS for 24h. $^{\#\#}p$<0.01 vs. the CN group; $^{**}p$<0.01 *vs.* the LPS group. CN: Control; NLRP3: NOD-like receptor thermal protein domain associated protein 3; IF: immunofluorescence; HNK: honokiol; LPS: lipopolysaccharide.

Significantly, the levels were observed to be reduced in the LPS+HNK group compared to the LPS group (p<0.01). These findings indicate significant differences between treatment groups.

HNK affected the expression of related proteins of NLRP3 inflammasome and Sirt1/autophagy axis in LPS-stimulated RAW 264.7 cells

WB analysis revealed the expression of NLRP3, Sirt1, Pro-IL-1β, Beclin-1 and LC3 II/LC3 I proteins. The results, presented in Figures 5D-5I, showed significant upregulation of all protein levels in the LPS group as compared to the CN group, except for Sirt1, which was downregulated by almost 45.3% (p<0.01). In contrast, the LPS+HNK group were reduced by 20.8% and 22.5% in NLRP3 and Pro-IL-1β proteins, respectively, as compared to the LPS group (p<0.05) (Fig. 5D,F). Furthermore, compared to the LPS group, the LPS+HNK group showed a 1.3-fold, 1.5-fold, and 3.3-fold increase in the levels of Sirt1, Beclin-1 and LC3 II/LC3 I, respectively (p<0.05) (Fig. 5E,G,H).

HNK inhibited the expression of NLRP3 in LPS-stimulated RAW 264.7 cells

Immunocytochemistry was used to assess the expression of NLRP3 in RAW 264.7 cells stimulated with LPS. The NLRP3 expression level was 2.33-fold higher in the LPS group compared to the CN group (p<0.01). In the LPS+HNK group, NLRP3 expression was reduced by 45% compared to the LPS group (p<0.01) (Fig. 6A,B).

HNK intervention antagonized the pro-inflammatory effect of NLRP3 overexpression in LPS-stimulated RAW 264.7 cells

Construction of NLRP3 overexpression cell lines was carried to investigate the effects of HNK regulation of NLRP3 in LPS-stimulated RAW 264.7 cells. In comparison to the LPS+EV group, the CD86 MFI were markedly decreased in the LPS+HNK group, while it was significantly increased in the LPS+NLRP3 group (p<0.01). Further, the MFI in the LPS+HNK+NLRP3 group were significantly lower than that in the LPS+NLRP3 groups (p<0.01) (Fig. 7A).

HNK inhibited the level of inflammation and affected the expression of related proteins of NLRP3 inflammasome and Sirt1/autophagy axis in LPS-stimulated RAW 264.7 cells via NLRP3

The mRNA levels of TNF-α, IL-1β and IL-6 in supernatant of cells overexpressing NLRP3 were measured using qRT-PCR. In the LPS and NLRP3 overexpression treated cells, the transcription levels of TNF-α, IL-1β and IL-6 mRNA were found to be significantly increased by more than 1.5-fold as compared to the LPS+EV group (p<0.01). On the other hand, the transcription levels of TNF-α, IL-1β and IL-6 were reduced by 14%, 18% and 34%, respectively, in the

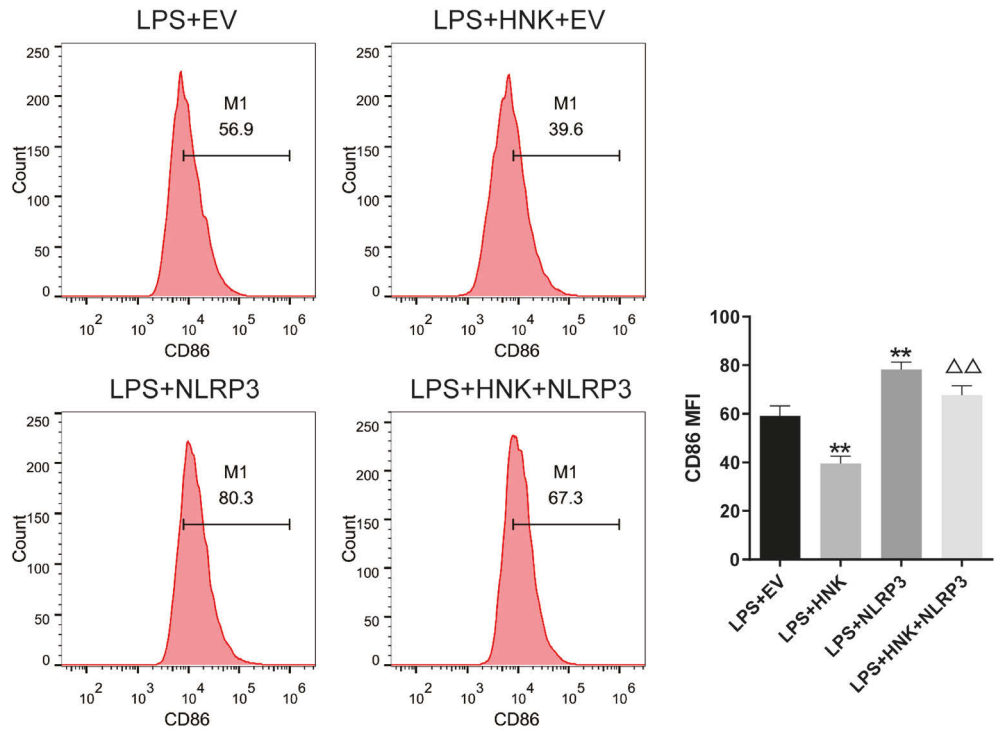

Fig. 7. HNK inhibited CD38 MFI in NLRP3 overexpression RAW 264.7 cells ($\bar{X}$±s, n=3). The CD38 MFI in RAW 264.7 cells were detected by flow cytometry. In the LPS+EV group, RAW 264.7 cells with the empty vector plasmid transfection were cultured for 24h with the LPS (10 μg/mL); In the LPS+HNK+EV group, RAW 264.7 cells with the empty vector plasmid transfection were cultured for 24h with the LPS and HNK (50 μM); In the LPS+NLRP3 group, the RAW 264.7 cell line with the NLRP3 overexpression, was treated with LPS for 24h; In the LPS+HNK+NLRP3 group performed the same operations as the LPS+NLRP3 group besides additional HNK pretreatment. *p<0.05, **p<0.01 *vs.* the LPS group; $^{\triangle\triangle}p$<0.01 *vs.* the LPS+NLRP3 group. NLRP3: NOD-like receptor thermal protein domain associated protein 3; HNK: honokiol; EV: empty vector; LPS: lipopolysaccharide; MFI: mean fluorescence intensity.

LPS+HNK+NLRP3 group as compared with the LPS+HNK+EV group (p<0.01) (Fig. 8A-C).

In addition, the protein expressions of NLRP3 inflammasome and Sirt1/autophagy axis in supernatant of NLRP3 overexpression cells was measured by WB. In the LPS+HNK+EV group, the levels of NLRP3 and Pro-IL-1β were reduced by nearly 23% compared to the LPS+EV group (p<0.05) (Fig. 8D,F), while the expression levels of Sirt1, Beclin-1 and LC3 II/LC3 I ratio were increased by 61%, 28% and 90%, respectively, compared to the LPS+EV group (Fig. 8E,G,H). Furthermore, compared with the LPS group, the LPS+NLRP3 group showed significantly increased levels of NLRP3 and Pro-IL-1β protein expression by 47% and 26.5% (p<0.05) (Fig. 8D,F). In the LPS+NLRP3 group, the Sirt1, Beclin-1, and LC3 II/LC3 I protein expression levels were reduced by approximately 48%, 36%, and 64%, respectively, compared to the LPS+EV group (p<0.01) (Fig. 8E,G,H). Remarkably, the protein expression levels of NLRP3 and Pro-IL-1β in the LPS+HNK+NLRP3 group were reduced by nearly 20% compared to that in the LPS+NLRP3 group (p<0.05) (Fig. 8D,F). On the contrary, contrasted to the LPS+NLRP3 group, the LPS+HNK+NLRP3 group exhibited a 2.19-fold, 1.52-fold, and 1.99-fold increase in expression levels of Sirt1, Beclin-1 and LC3 II/ LC3 I proteins, respectively (p<0.05 or p<0.01) (Fig. 8E,G,H).

Discussion

AP is characterized by a high incidence rate and mortality (Pörner et al., 2021). Thus, effective prevention and treatment methods are essential. CLP surgery usually cause organ injury with a poor survival rate to establish a common experiment model *in vivo* for AP (Toscano et al., 2011). This study induced AP in rats through CLP surgery and observed acute inflammation and bacterial infection. Remarkably, HNK treatment improved the survival rate, ameliorated the lung and

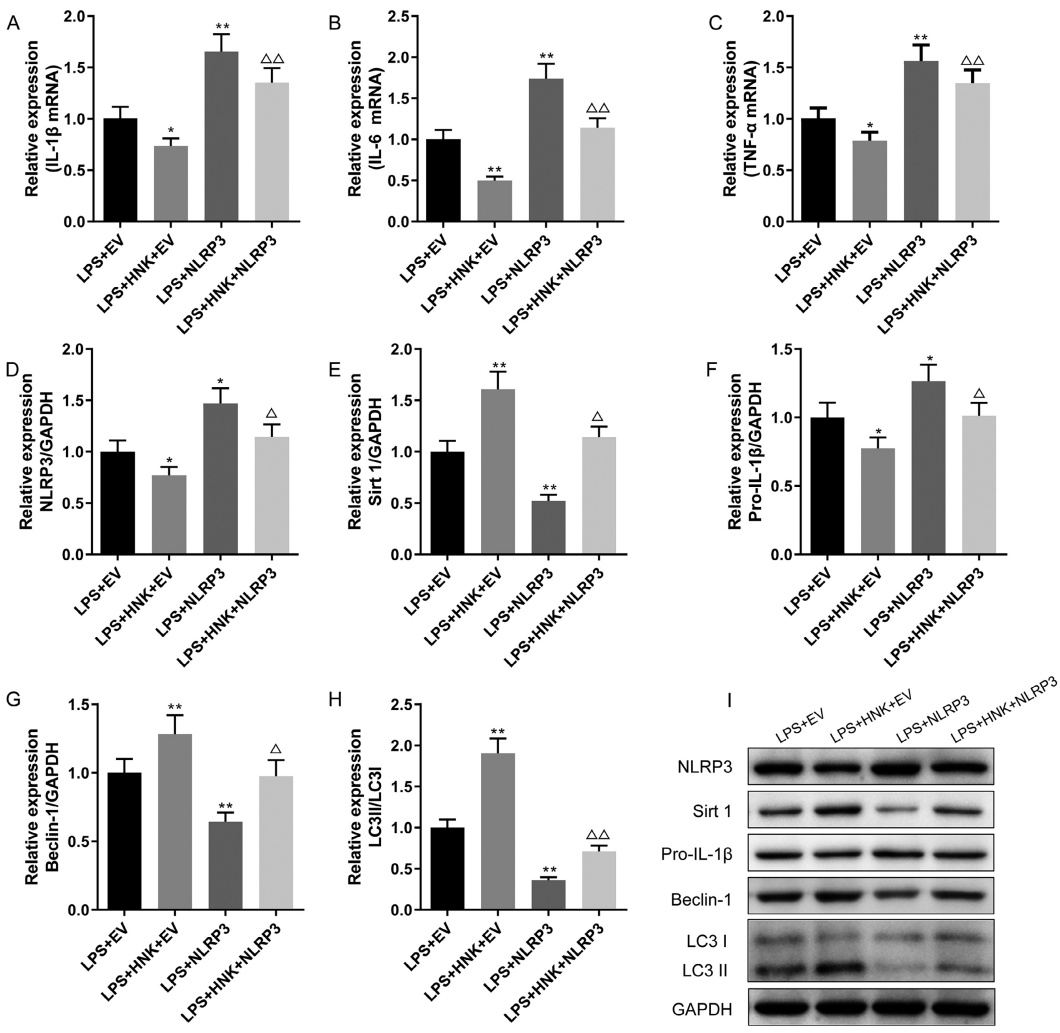

Fig. 8. The levels of TNF-α, IL-1β and IL-6 mRNA and related proteins of NLRP3 inflammasome and Sirt1/autophagy axis in NLRP3-overexpressed RAW 264.7 cells. ($\bar{X}$±s, n=3). **A-C.** The levels of TNF-α, IL-1β and IL-6 mRNA were measured by quantitative real-time PCR. **D-I.** The levels of NLRP3, Sirt1, Pro-IL-1β, Beclin-1, and LC3 II/LC3 I proteins were measured by Western blot. The LPS+EV group, RAW 264.7 cells with the empty vector plasmid transfection were cultured for 24h with the LPS (10 μg/mL); The LPS+HNK+EV group, RAW 264.7 cells with the empty vector plasmid transfection were cultured for 24h with the LPS and HNK (50 μM); the LPS+NLRP3 group, the RAW 264.7 cell line with the NLRP3 overexpression, was treated with LPS for 24h. The LPS+HNK+NLRP3 group performed the same operations as the LPS+NLRP3 group besides additional HNK (50 μM) pretreatment. *p<0.05, **p<0.01 vs. the LPS group; $^{\Delta}p$<0.05, $^{\Delta\Delta}p$<0.01 *vs.* the LPS+NLRP3 group. TNF-α: Tumor necrosis factor-α; IL: Interleukin; NLRP3: NOD-like receptor thermal protein domain associated protein 3; Sirt1: Sirtuin1; LC3: MAP1LC3; HNK: honokiol; LPS: lipopolysaccharide; EV: empty vector.

kidney injury, and reduced serum biochemical indexes. Specifically, HNK treatment markedly reduced inflammatory infiltration in the lung and kidney and protected against AP-induced damage. In conclusion, this study suggests that HNK may serve as a potential therapeutic option for AP.

Serious increases in proinflammatory factors during AP can result in significant damage to organ and even death (Seemann et al., 2017). Studies have shown that inhibiting the levels of TNF-α, IL-1β, and IL-6 can effectively improve AP (Panpetch et al., 2018; Zhao et al., 2020). Similarly, the NLRP3 inflammasome, which plays a crucial role in the innate immune system, drives the assembly and release of IL-1β and IL-18 in response to microbial infection and cellular damage (Kelley et al., 2019). Liu and colleagues reported that buformin can alleviate acute sepsis-induced lung injury by inhibiting NLRP3 (Liu et al., 2022a). Therefore, this study aimed to investigate the effect of HNK on NLRP3 inflammasome and inflammation in CLP rats and RWA 264.7 cells, and found that HNK treatment improves cellular inflammation by regulating NLRP3. Moreover, immunosuppression is observed in CLP rats (Markwart et al., 2014) and this study found that $CD4^+$ and $CD8^+$ T cells decreased significantly in CLP rats. Studies have shown that rats with regulatory T cells have a better prognosis for sepsis recovery (Kühlhorn et al., 2013). In this study, HNK treatment increased the T cell levels in CLP rats and activated their immune capacity. Furthermore, this study demonstrated that HNK improved immunity and inflammation by inhibiting NLRP3 inflammasome suggesting the importance of NLRP3 inflammasome in HNK improvement in AP.

Additionally, autophagy was inhibited in CLP rats while HNK treatment promoted autophagy and improved AP. Studies have suggested a vital role of autophagy in protecting against infections and endogenous sources of inflammation (Deretic, 2021). This study discovered that HNK treatment reduced bacterial infection levels in the blood and peritoneal fluid of CLP rats. Sirt1 activation has been shown to ameliorate acute kidney injury, cardiac dysfunction, and lung injury in sepsis (Zhang et al., 2019; Chen et al., 2020; Deng et al., 2021). Recent studies indicate that Sirt1 can inhibit inflammation and apoptosis through activating autophagy, which is mainly achieved by lysosomal degradation of cytoplasmic autophagy via autophagy protein LC3 (Xu et al., 2020; Ma et al., 2021). Acetylation at the autophagy-related Beclin-1-PIK3C3 complex has surfaced as a pivotal regulatory mechanism for autophagy (Xu and Wan, 2023). Acetyltransferases EP300 can suppress the activity of this complex and autophagy induction by acetylating PIK3C3 and BECN1 (Sun et al., 2015). Sirt1 inhibits Beclin-1 acetylation (Deng et al., 2021) and removes the acetyl group from the acetylated lysine residues of ATG5, ATG7, and LC3. ATG5 and ATG7 are involved in the formation of membrane-bound LC3-phosphatidylethanolamine (PE), a vital event of autophagy (Huang et al., 2015). In conclusion, Sirt1 deacetylates Beclin1, ATG5, ATG7, and LC3 to enhance autophagy. In line with this, this study found that HNK treatment of RAW 264.7 cells was linked to Sirt1/Beclin-1/LC3 in regulating inflammation. Autophagy has been proved to balance immunity (Deretic et al., 2013). In this study, HNK treatment of LPS-induced cells with NLRP3 overexpression still activated the Sirt1/Beclin-1/LC3 pathway implying that HNK could enhance immunity and inhibit inflammation via Sirt1 autophagy to improve AP. The regulation of the Sirt1 autophagy axis by HNK merits further exploration. This study provides a foundation and direction for AP treatment and drug development.

This study found that HNK can improve infection, inflammation and immunity in AP, while also inhibiting inflammatory phenotype in macrophages. Furthermore, it demonstrated that HNK improved cell inflammation and immunity by inhibiting NLRP3 and activating the Sirt1 autophagy axis. However, this study has not yet demonstrated the direct interaction between HNK and Sirt1, and further research is needed to investigate the intermediate process of how HNK regulates NLRP3 and Sirt1. In conclusion, this study confirms the potential of HNK intervention in the treatment of AP and provides a scientific basis for the application of HNK.

Acknowledgements. None.

Conflict of interest statement. There is no conflict of interest between the authors of this article.

References

Boland C., Collet V., Laterre E., Lecuivre C., Wittebole X. and Laterre P.F. (2011). Electrical vagus nerve stimulation and nicotine effects in peritonitis-induced acute lung injury in rats. Inflammation 34, 29-35.

Chakraborty R.K. and Burns B. (2022). Systemic inflammatory response syndrome. StatPearls. Treasure Island (FL), StatPearls Publishing; 2023 Jan. 2023 May 29.

Chen S., Ding R., Hu Z., Yin X., Xiao F., Zhang W., Yan S. and Lv C. (2020). MicroRNA-34a inhibition alleviates lung injury in cecal ligation and puncture induced septic mice. Front. Immunol. 11, 1829.

Chiu K.C., Shih Y.H., Wang T.H., Lan W.C., Li P.J., Jhuang H.S., Hsia S.M., Shen Y.W., Yuan-Chien Chen M. and Shieh T.M. (2021). *In vitro* antimicrobial and antipro-inflammation potential of honokiol and magnolol against oral pathogens and macrophages. J. Formosan Med. Assoc. 120, 827-837.

Deng Z., Sun M., Wu J., Fang H., Cai S., An S., Huang Q., Chen Z., Wu C., Zhou Z., Hu H. and Zeng Z. (2021). SIRT1 attenuates sepsis-induced acute kidney injury via Beclin1 deacetylation-mediated autophagy activation. Cell Death Dis. 12, 217.

Deretic V. (2021). Autophagy in inflammation, infection, and immunometabolism. Immunity 54, 437-453.

Deretic. V., Saitoh. T. and Akira. S. (2013). Autophagy in infection, inflammation and immunity. Nat. Rev. Immunol. 13, 722-737.

Doklestić S.K., Bajec D.D., Djukić R.V., Bumbaširević V., Detanac A.D., Detanac S.D., Bracanović M. and Karamarković R.A. (2014). Secondary peritonitis - evaluation of 204 cases and literature review. J. Med. Life 7, 132-138.

Hautem N., Morelle J., Sow A., Corbet C., Feron O., Goffin E., Huaux F.

and Devuyst O. (2017). The NLRP3 Inflammasome has a critical role in peritoneal dialysis-related peritonitis. J. Am. Soc. Nephrol. 28, 2038-2052.

Huang R., Xu Y., Wan W., Shou X., Qian J., You Z., Liu B., Chang C., Zhou T., Lippincott-Schwartz J. and Liu W. (2015). Deacetylation of nuclear LC3 drives autophagy initiation under starvation. Mol. Cell 57, 456-466.

Jiao Y., Zhang T., Zhang C., Ji H., Tong X., Xia R., Wang W., Ma Z. and Shi X. (2021). Exosomal miR-30d-5p of neutrophils induces M1 macrophage polarization and primes macrophage pyroptosis in sepsis-related acute lung injury. Crit. Care 25, 356.

Kelley N., Jeltema D., Duan Y. and He Y. (2019). The NLRP3 inflammasome: An overview of mechanisms of activation and regulation. Int. J. Mol. Sci. 20, 3328.

Kolaczkowska E., Koziol A., Plytycz B. and Arnold B. (2010). Inflammatory macrophages, and not only neutrophils, die by apoptosis during acute peritonitis. Immunobiology 215, 492-504.

Kühlhorn F., Rath M., Schmoeckel K., Cziupka K., Nguyen H.H., Hildebrandt P., Hünig T., Sparwasser T., Huehn J., Pötschke C. and Bröker B.M. (2013). Foxp3$^+$ regulatory T cells are required for recovery from severe sepsis. PLoS One 8, e65109.

Li Y., Liang C. and Zhou X. (2022). The application prospects of honokiol in dermatology. Dermatol. Ther. 35, e15658.

Liu B., Wang Z., He R., Xiong R., Li G., Zhang L., Fu T., Li C., Li N. and Geng Q. (2022a). Buformin alleviates sepsis-induced acute lung injury via inhibiting NLRP3-mediated pyroptosis through an AMPK-dependent pathway. Clin. Sci. (Lond) 136, 273-289.

Liu J., Wu Y.H., Zhang Z.L. and Li P. (2022b). Tanshinone IIA improves sepsis-induced acute lung injury through the ROCK2/NF-κB axis. Toxicol. Appl. Pharmacol. 116021.

Ma C., Zhang D., Ma Q., Liu Y. and Yang Y. (2021). Arbutin inhibits inflammation and apoptosis by enhancing autophagy via SIRT1. Adv. Clin. Exp. Med., 30, 535-544.

Markwart R., Condotta S.A., Requardt R.P., Borken F., Schubert K., Weigel C., Bauer M., Griffith T.S., Förster M., Brunkhorst F.M., Badovinac V.P. and Rubio I. (2014). Immunosuppression after sepsis: systemic inflammation and sepsis induce a loss of naïve T-cells but no enduring cell-autonomous defects in T-cell function. PLoS One 9, e115094.

Metur S.P. and Klionsky D.J. (2021). Adaptive immunity at the crossroads of autophagy and metabolism. Cell. Mol. Immunol. 18, 1096-1105.

Mikhalchik E.V., Borodina I.V., Vlasova I.V., Vakhrusheva T.V., Gorbunov N.P., Panasenko O.M., Titkova S.M., Anurov M.V., Ivakhov G.B., Ermakov I.V., Teplyshev A.V. and Klinov D.V. (2020). Biomarkers of system inflammation in local and diffuse peritonitis. Biomed. Khim. 66, 411-418 (in Russian).

Nurmi K., Kareinen I., Virkanen J., Rajamäki K., Kouri V.P., Vaali K., Levonen A.L., Fyhrquist N., Matikainen S., Kovanen P.T. and Eklund K.K. (2017). Hemin and cobalt protoporphyrin inhibit NLRP3 inflammasome activation by enhancing autophagy: A novel mechanism of inflammasome regulation. J. Innate Immun. 9, 65-82.

Panpetch W., Chancharoenthana W., Bootdee K., Nilgate S., Finkelman M., Tumwasorn S. and Leelahavanichkul A. (2018). *Lactobacillus rhamnosus* L34 attenuates gut translocation-induced bacterial sepsis in murine models of leaky gut. Infect. Immun. 86, e00700-00717.

Pörner D., Von Vietinghoff S., Nattermann J., Strassburg C.P. and Lutz P. (2021). Advances in the pharmacological management of bacterial peritonitis. Expert Opin. Pharmacother. 22, 1567-1578.

Rodrigues F.A.P., Santos A., De Medeiros P., Prata M.M.G., Santos T.C.S., Da Silva J.A., Brito G.A.C., Dos Santos A.A., Silveira E.R., Lima AÂ M. and Havt A. (2018). Gingerol suppresses sepsis-induced acute kidney injury by modulating methylsulfonylmethane and dimethylamine production. Sci. Rep. 8, 12154.

Seemann S., Zohles F. and Lupp A. (2017). Comprehensive comparison of three different animal models for systemic inflammation. J. Biomed. Sci. 24, 60.

Sun T., Li X., Zhang P., Chen W.D., Zhang H.L., Li D.D., Deng R., Qian X.J., Jiao L., Ji J., Li Y.T., Wu R.Y., Yu Y., Feng G.K. and Zhu X.F. (2015). Acetylation of Beclin 1 inhibits autophagosome maturation and promotes tumour growth. Nat. Commun. 6, 7215.

Toscano M.G., Ganea D. and Gamero A.M. (2011). Cecal ligation puncture procedure. J. Vis. Exp. 7, 2860.

Wang W., Wang Z., Yang X., Song W., Chen P., Gao Z., Wu J. and Huang F. (2022). Rhein ameliorates septic lung injury and intervenes in macrophage metabolic reprogramming in the inflammatory state by Sirtuin 1. Life Sci. 310, 121115.

Wu C.Y., Hua K.F., Yang S.R., Tsai Y.S., Yang S.M., Hsieh C.Y., Wu C.C., Chang J.F., Arbiser J.L., Chang C.T., Chen A. and Ka S.M. (2020). Tris DBA ameliorates IgA nephropathy by blunting the activating signal of NLRP3 inflammasome through SIRT1- and SIRT3-mediated autophagy induction. J. Cell. Mol. Med. 24, 13609-13622.

Xia S., Lin H., Liu H., Lu Z., Wang H., Fan S. and Li N. (2019). Honokiol attenuates sepsis-associated acute kidney injury via the inhibition of oxidative stress and inflammation. Inflammation 42, 826-834.

Xu Y. and Wan W. (2023). Acetylation in the regulation of autophagy. Autophagy 19, 379-387.

Xu C., Wang L., Fozouni P., Evjen G., Chandra V., Jiang J., Lu C., Nicastri M., Bretz C., Winkler J.D., Amaravadi R., Garcia B.A., Adams P.D., Ott M., Tong W., Johansen T., Dou Z. and Berger S.L. (2020). SIRT1 is downregulated by autophagy in senescence and ageing. Nat. Cell Biol. 22, 1170-1179.

Yang S.R., Hsu W.H., Wu C.Y., Shang H.S., Liu F.C., Chen A., Hua K.F. and Ka S.M. (2020). Accelerated, severe lupus nephritis benefits from treatment with honokiol by immunoregulation and differentially regulating NF-κB/NLRP3 inflammasome and sirtuin 1/autophagy axis. FASEB J. 34, 13284-13299.

Youm Y.H., Nguyen K.Y., Grant R.W., Goldberg E.L., Bodogai M., Kim D., D'agostino D., Planavsky N., Lupfer C., Kanneganti T.D., Kang S., Horvath T.L., Fahmy T.M., Crawford P.A., Biragyn A., Alnemri E. and Dixit V.D. (2015). The ketone metabolite β-hydroxybutyrate blocks NLRP3 inflammasome-mediated inflammatory disease. Nat. Med. 21, 263-269.

Zhang M. and Shen Y. (2021). Research advances on anti-inflammation and their mechanisms of extract, magnolol and honokiol from Magnoliae Officinalis Cortex. Drug Evaluation Res. 44, 2739-2746 (in Chinese).

Zhang W.X., He B.M., Wu Y., Qiao J.F. and Peng Z.Y. (2019). Melatonin protects against sepsis-induced cardiac dysfunction by regulating apoptosis and autophagy via activation of SIRT1 in mice. Life Sci. 217, 8-15.

Zhao J., Chen Y., Dong L., Li X., Dong R., Zhou D., Wang C., Guo X., Zhang J., Xue Z., Xi Q., Zhang L., Yang G., Li Y. and Zhang R. (2020). Arctigenin protects mice from thioglycollate-induced acute peritonitis. Pharmacol. Res. Perspect. 8, e00660.

Accepted December 12, 2023